Materials Research. 2025; 28: e20250150
DOI: https://doi.org/10.1590/1980-5373-MR-2025-0150

Effect of CaO and ZnO Additions on Density, Electrical, and Thermal Properties of Gd-Doped Ceria

***G. Martínez-De la Rosa*[a], *J.A. Díaz-Guillén*[a*], *O.J. Durá*[b], *M.E. Bazaldúa-Medellín*[c], *O. Burciaga-Díaz*[a], *K.P. Padmasree*[d]**

[a]*Tecnológico Nacional de México, Instituto Tecnológico de Saltillo, Blvd. Venustiano Carranza, 2400, 25280, Saltillo, México.*
[b]*Universidad de Castilla-La Mancha, Escuela Técnica Superior de Ingeniería Industrial, Departamento de Física, 13071, Ciudad Real, España.*
[c]*Universidad Autónoma de Coahuila, Facultad de Ingeniería, 25354, Arteaga, México.*
[d]*Centro de Investigación y de Estudios Avanzados (CINVESTAV), Unidad Saltillo, 25900, Ramos Arizpe, México.*

Received: January 13, 2025; Revised: April 03, 2025; Accepted: May 14, 2025

The effects of CaO and ZnO as sintering aids on the electrical and thermal properties of Gd-doped CeO_2 ceramics were investigated. Different systems of general formulas $Gd_{0.1}Ce_{0.9}O_{1.95}$ and $A_{0.02}Gd_{0.08}Ce_{0.9}O_{1.94}$ (where A = Ca and Zn) were obtained by mechanochemistry, with a maximum milling time of 20 h. XRD analysis of synthesized samples revealed pure phases with a fluorite-type structure, derived from the CeO_2 cubic system. Heat treatments from 800 to 1500°C enhanced crystallinity and confirmed the formation of the solid solution. SEM studies of samples sintered at 1200 and 1350°C showed similar characteristics across all systems. Both CaO and ZnO improved the materials' relative density (~95%) at a sintering temperature of 1200 °C. Impedance spectroscopy demonstrated that the sintering aids did not have an adverse effect on ionic conductivity at 650°C, while thermal conductivity tended to decrease as the temperature increased, aligning with density results.

Keywords: *SOFC, Gd-doped ceria, solid electrolytes, mechanochemistry, sintering aids, thermal barrier coatings.*

1. Introduction

Solid oxide fuel cells (SOFC) represent an innovative approach to generating electrical energy aimed at decarbonizing the environment. They provide high-efficiency methods for producing electricity through reactions between hydrogen fuel and oxygen[1]. These cells consist of an anode, a cathode, and a solid electrolyte, the latter of interest for this research. The 8YSZ (8% molar yttria-stabilized zirconia) is the most commonly used electrolyte at operating temperatures of 700 to 1000 °C [2]. These conditions eventually lead to the degradation of cell materials, either through microstructural alterations that result in fractures and delamination or through external factors like corrosion or reactions with fuel gas, which undermine the performance of the SOFC[3]. This is why materials such as doped ceria have gained significance in reducing the operating temperature of SOFCs to below 650 °C, resulting in Low-Temperature SOFCs (LT-SOFCs).

On the other hand, thermal barrier coatings (TBCs) are systems designed to thermally insulate metallic substrates exposed to high temperatures and harsh environments by applying thin ceramic layers. These coatings reduce the internal temperature of machinery, enabling higher operating temperatures, improved efficiency, and extended service life. The ceramic materials used for these coatings must possess specific properties, including low thermal conductivity (below 3 W/m K), a high coefficient of thermal expansion (CTE), excellent thermal and chemical stability, and strong mechanical resistance. The most commonly used material for TBCs is zirconia partially stabilized with 4–4.6 molar % yttria (YPSZ). However, it has some drawbacks, such as its tendency to densify at temperatures around 1200 °C, which reduces porosity and consequently increases thermal conductivity[4,5].

Ceria doped with divalent, trivalent, or pentavalent elements such as Sm, Gd, Dy, Ca, Mn, and others[6-12] has shown promising properties for various applications, including spintronics, photocatalysis, and gas sensors[13,14]. However, its most notable applications are in SOFCs and TBCs, which constitute the primary focus of this research. However, it still has some limitations, requiring high sintering temperatures to attain adequate densification. Processing the material under these conditions results in chemical changes such as reduction from Ce^{+4} to Ce^{+3}, thus leading to a reduction in the cell's electrical efficiency due to the electronic conduction arising from this conversion[8,9]. Various investigations have been focused on promoting the densification of doped ceria at lower sintering temperatures through different synthesis methods[15,16] or chemical compositions[17,18], indirectly affecting ionic conductivity.

This research uses a novel approach by utilizing divalent sintering aids, such as Ca and Zn, to simultaneously enhance oxygen vacancy concentration and densification. This innovative strategy optimizes density in Gd-doped ceria while maintaining the high ionic conductivity and low thermal conductivity essential for LT-SOFCs and TBCs.

*e-mail: jose.dg@saltillo.tecnm.mx

Furthermore, high-energy mechanical milling as a synthesis method enables the production of highly structurally disordered ceramics at room temperature, activating the material for the sintering process, thereby lowering the required sintering temperature[19]. Mechanical milling is an effective method for synthesizing compounds, solid solutions, and new crystalline phases through solid-state reactions, which typically require high temperatures[20,21]. However, high-energy milling, such as planetary or vibratory mills, enables these reactions to occur at room temperature. This technique provides precise control over material properties by introducing structural defects that are difficult to achieve with other methods. The resulting materials often have a metastable state, structural disorder, and high vacancy concentrations, making them ideal for developing SOFC electrolytes.

These characteristics may also improve the materials' thermal insulation properties, making them well-suited for a variety of applications.

2. Materials and Methods

Systems with the general formulas $Gd_{0.1}Ce_{0.9}O_{1.95}$ and $A_{0.02}Gd_{0.08}Ce_{0.9}O_{1.94}$ (where A = Ca and Zn) were synthesized using mechanochemistry. The starting materials—CeO_2, Gd_2O_3, ZnO, and CaO powders (Sigma-Aldrich, 99.9% purity)—were processed in a high-energy planetary mill (RETSCH PM100) at 400 rpm for up to 20 hours. Heat treatments were subsequently performed at 800, 1000, 1200, 1350, and 1500 °C. The selected maximum milling time and sintering temperatures were based on prior studies[22].

The crystalline structure evolution of the systems, influenced by milling time and heat treatment temperature, was characterized via X-ray diffraction (XRD) using a Rigaku IV diffractometer. This utilized Cu Kα radiation λ=1.54 Å with operating conditions of 30 mA current and 40 kV voltage. XRD data were also used to calculate the lattice parameter using Bragg's Law $n\lambda=2d \sin\theta$, and the equation $a_0=d/[(h)^2+(k)^2+(l)^2]^{½}$.

Powders of each composition were pressed uniaxially at 550 MPa and sintered for 6 hours at 1200 °C and 1350 °C. Their morphologies were analyzed using a field emission scanning electron microscope (FE-SEM, TESCAN-MIRA 3) with secondary electron mode under an accelerating voltage of 20 kV, beam intensity index 9, working distance of 12 mm, and spot size of 40 nm.

The relative density was determined by comparing the theoretical density, calculated from the lattice parameter obtained via XRD, with the experimental density measured using the Archimedes method.

Impedance spectroscopy was conducted on samples sintered at 1200 °C. The samples were coated with silver paint on both sides and subjected to a heat treatment at 700 °C for 2 hours to remove organic components, enabling the silver paint to function as blocking electrodes. Measurements were performed from 300 to 650 °C using a Solartron 1260 Frequency Response Analyzer (FRA) with a custom-built sample holder and furnace.

Thermal conductivity (k) at various temperatures was calculated using the equation $k = \alpha \cdot \rho \cdot C_p$, where α is the thermal diffusivity measured via the laser flash method (Linseis LFA 1000, under Ar atmosphere), C_p is the specific heat determined using a Netzsch Jupiter DSC 404 differential scanning calorimeter, and ρ is the experimental density.

3. Results

The XRD patterns of sample Ca- GDC with composition $Ca_{0.02}Gd_{0.08}Ce_{0.9}O_{1.94}$ at different milling times and heat treated at different temperatures are presented in Figure 1. Their respective references from the International Centre for Diffraction Data (ICDD) are included as well for comparison purposes. This figure represents all the systems. At 0 hours of milling as shown in Figure 1(a), and according to the reported pattern in ICDD, the signals for ceria and gadolinia appear as sharp and prominent peaks. With an increase in milling time, only the broadened peaks typical of the cubic fluorite-type structure of ceria can be observed, indicating the incorporation of Gd and Ca into the structure. The reflections become wider and less intense due to the structural disorder introduced during mechanical milling. Likewise, it is shown that raising the heat treatment temperature results in the peaks becoming sharper and more intense, which is attributed to the enhanced crystalline order of the solid solution. These findings demonstrate the effectiveness of mechanical milling in producing the proposed compositions, confirming the absence of starting reagents after 20 hours of milling, followed by heat treatments at temperatures reaching up to 1500°C. The prevailing structures in all cases correspond fundamentally to phases similar to cubic fluorite, characteristic of CeO_2.

In Figure 2 (a) the XRD patterns of all systems after 1350 °C heat treatment with their lattice parameters are found. A common issue in synthesis through mechanical milling is product contamination from the mortar or milling media (in

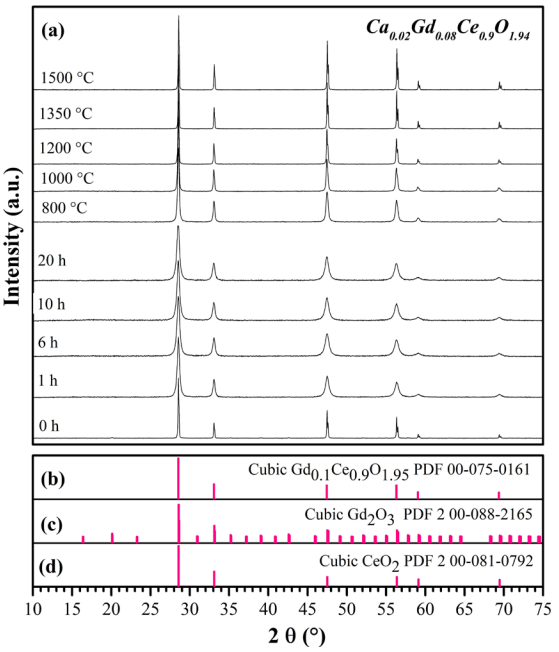

Figure 1. XRD pattern of the sample Ca-GDC. (a) Milled from 0 to 20 h and heat treated at 800, 1000, 1200, 1350, and 1500 °C; (b) (c) and (d) are the reported ICDD patterns for $Gd_{0.1}Ce_{0.9}O_{1.95}$, cubic Gd_2O_3, and cubic CeO_2, respectively.

this case, zirconia balls), which can occur due to the constant collisions of materials. However, none of the three systems depicted in the image show any signals of secondary phases related to contamination from milling, dopant elements, or sintering additives. All patterns are consistent with that of the ceria reported by ICDD (Figure 2(b)), confirming the formation of the ceria solid solutions. On the other hand, in the lattice parameters (a_0), it is observed that this value increases slightly in the doped systems, this difference may be originated from the partial substitution of the Ce^{+4} ions (r_{Ce} (VIII)= 0.97 Å) by ions of larger radius such as Gd^{+3} (r_{Gd} (VIII)= 1.053 Å)[23]. This observation indicates the necessity of preserving a neutral ionic charge within the crystalline structure, which leads to the creation of oxygen vacancies when tetravalent atoms are replaced by trivalent ones.

This process is described with the following reaction:

$$(1/2\gamma Gd_2O_3) + (1-\gamma CeO_2) \rightarrow Gd_\gamma Ce_{1-\gamma}O_{2-\delta} \quad (1)$$

Where δ denotes the quantity of oxygen that has exited the system and will increase with lower valence ions. The vacancies created facilitate ionic conduction within the material through vacancy migration, leading to improved electrical properties at lower temperatures.

Figure 3 represents the typical morphology of pellets of pure GDC, with Ca, and Zn milled for 20 h and sintered at temperatures of 1200 and 1350 °C for 6 h analyzed by FE-SEM. In all instances, the results indicate that the systems sintered at 1350 °C exhibit well-defined grains with a polygonal morphology and irregular sizes, as well as clean and clearly defined grain boundaries. In contrast, the grains of the samples sintered at 1200 °C predominantly display a semi-globular morphology, along with substantial residual porosity between the grains that have not fully developed. There is no notable difference between the micrographs of the compositions with sintering aids and those without. It is important to mention that, only pellets sintered at a maximum temperature of 1350 °C were analyzed, since above this temperature, they showed bubble formation, cracks, and even broke completely. This behavior has been associated by some authors to the ceria reduction reaction from CeO_2 to Ce_2O_3 at temperatures around 1500 °C (or under reducing conditions)[24-26]. This reaction usually leads to an outflow of oxygen, and therefore to a cracked material.

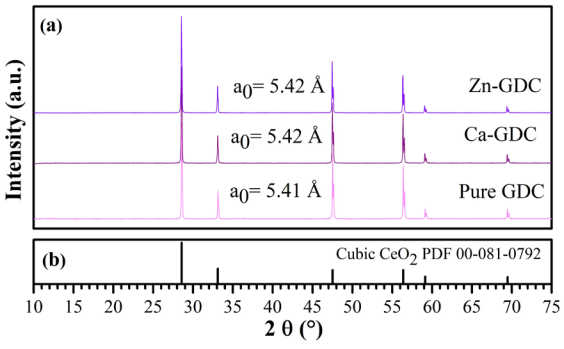

Figure 2. (a) XRD patterns of all studied systems fired at 1350 °C; (b) Reported ICDD pattern for cubic CeO_2.

The relative densities are shown in Table 1. Here it is observed that at 1200 °C the relative density of the systems with the incorporation of sintering aids, both Ca and Zn, was higher than the pure sample. This confirms that incorporating these elements into the ceria structure promotes densification at lower temperatures. At 1350 °C the density percentage increases for the pure sample and the one with Ca, while the one with Zn decreases. The highest density value was that of Zn-GDC sintered at 1200 °C.

Impedance spectroscopy results are represented in Figure 4. A plot of the dependence of conductivity (σ) on frequencies of 100 Hz- 1 MHz and temperatures between 300 and 650 °C on a double logarithmic scale of the system Ca-GDC representing all the systems can be found in (a). The increase in frequencies of electrical stimuli applied to the material is reflected in the increase in electrical conductivity. This behavior was termed Universal Dynamic Response (UDR) by A.K. Jonscher in 1983[27] and is representative of predominantly ionic conductors. Lower frequencies represent longer conduction times in which the ions have

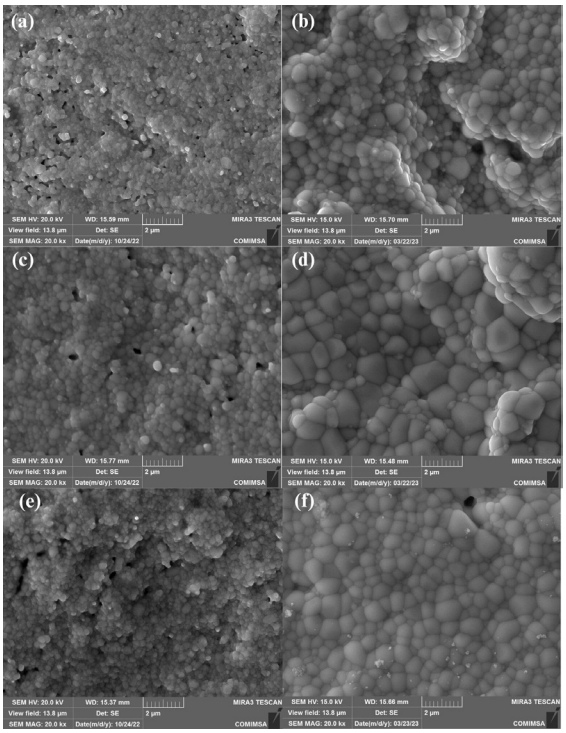

Figure 3. FE-SEM images at 20kX magnification showing the microstructures of: (a) pure GDC sintered at 1200 °C, (b) pure GDC sintered at 1350 °C, (c) Ca-GDC sintered at 1200 °C, (d) Ca-GDC sintered at 1350 °C, (e) Zn-GDC sintered at 1200 °C, and (f) Zn-GDC sintered at 1350 °C.

Table 1. Relative densities of doped ceria systems sintered at 1200 and 1350 °C.

Sample	Relative density (%)	
	1200 °C	1350 °C
$Gd_{0.1}Ce_{0.9}O_{1.95}$ (pure)	89	95.16
$Ca_{0.02}Gd_{0.08}Ce_{0.9}O_{1.94}$	94.26	95.31
$Zn_{0.02}Gd_{0.08}Ce_{0.9}O_{1.94}$	95.64	89.54

the opportunity to interact with each other, perform long-range movements, and even reach the grain boundaries of the material, areas that act as barriers to them causing a decrease in conductivity values. Meanwhile, at high frequencies, the ions only move to nearby sites. The dc or bulk conductivity (σ_{dc}) is shown as a plateau where the conductivity is constant with frequency. These results are distant from Debye's ideal response, corroborating that the conductivity of the material is essentially ionic. As for the application of temperature, it can be seen that it causes the increase of σ_{dc}. This dependence can be studied if an Arrhenius-type representation is made as in Figure 4(d) which follows the following equation:

$$\sigma_{dc}T = \sigma_0 exp\left(-E_{dc} / K_bT\right) \quad (2)$$

where σ_0 is the pre-exponential factor proportional to the number of mobile charge carriers, and E_{dc} is the activation energy for oxygen ion migration. The straight lines are the result of fitting the data, so it can be said that the process is thermally activated.

Nyquist plots at 350 °C of all systems sintered at 1200 °C are shown in Figure 4(b). Semicircles representing the grain boundary contribution can be observed, followed by a tail at high frequencies that corresponds to the electrode contribution, a feature typical of ionic conductive materials[28]. The GDC and Zn-GDC compositions present similar diameters, while the Ca-GDC system has a smaller diameter indicating a higher conductivity at this temperature, however, as shown in the previous figures, at 650 °C there is no significant difference in conductivity in all systems.

Figure 4(c) illustrates the blocking effects in these materials by showing the dielectric permittivity as a function of temperature and frequency on a logarithmic scale for the representative Ca-GDC composition. The increase in permittivity at low frequencies is attributed to the blocking effects of ions at grain boundaries and electrodes, highlighting the predominantly ionic nature of these materials. These results indicate that the sintering aids enhanced material densification at lower sintering temperatures, such as 1200 °C, without compromising ionic conductivity. Furthermore, the conductivity values are comparable to those reported in the literature for similar compositions, as shown in Table 2.

Finally, Figure 4(e) summarizes the conductivities and activation energies at 650 °C with the composition of the systems. Ionic conductivities of 8.48×10^{-2}, 5.69×10^{-2}, and 6.52×10^{-2} S/cm were found for the pure system, Ca, and Zn, respectively. The incorporation of sintering aids in the structure did not affect the conductivity and the activation energy of the material, as the range of values was very similar for all compositions.

There was a tendency for all materials to decrease their thermal conductivity with increasing temperature between 100 and 300 °C followed by almost constant values, some of them with a slight increase related to radiation heat transfer, as shown in Figure 5 (a) and (b). This is an important characteristic of non-metallic inorganic materials since an increase in temperature also means higher vibrational energy and probability of phonon scattering. The Ca-GDC composition sintered at 1350 °C obtained the lowest thermal

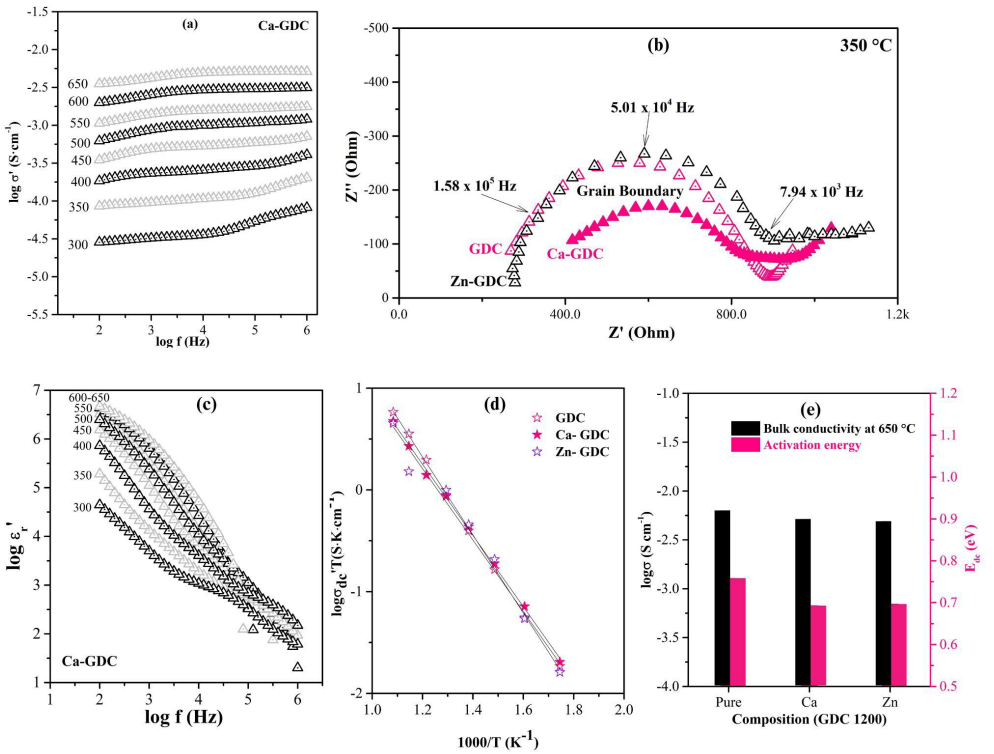

Figure 4. (a) Representative plot of conductivity vs. frequency at various temperatures (°C) for the Ca-GDC system sintered at 1200 °C, presented on a double logarithmic scale; (b) Impedance spectra for all systems at 350 °C; (c) Real part of electrical permittivity as a function of temperature and frequency for the Ca-GDC system; (d) Arrhenius plot of the bulk conductivity for all compositions, with the straight line representing the best fit to the data; (e) Direct current conductivity (σ_{dc}) and activation energies (E_{dc}) at 650 °C for each composition.

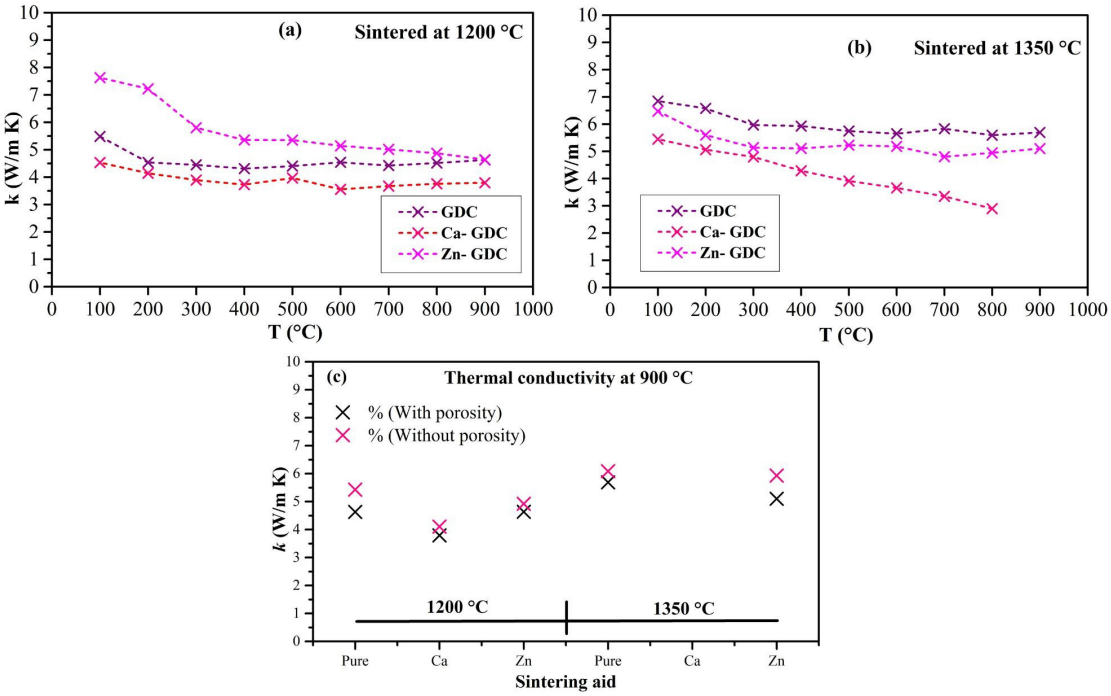

Figure 5. Thermal conductivity (k) as a function of temperature of samples (a) sintered at 1200 °C and (b) 1350 °C. Comparison of the termal conductivity at 900 °C of each system according to the effect of porosity (c).

Table 2. Conductivities (σ), activation energies (E_{dc}), and relative densities of similar compositions of doped ceria.

Composition	Sintering	Relative density (%)	σ (S/cm)	E_{dc} (eV)	Ref.
$Ce_{0.89}La_{0.07}Sr_{0.04}O_{1.925}$	1350 °C for 4 h	95	2.370×10^{-2} (600 °C)	0.91	[29]
$Ce_{0.88}Gd_{0.06}Pr_{0.06}O_2$	1300 °C for 10 h	≥98	1.712×10^{-2} (600 °C)	0.77	[30]
$Ce_{0.8}Sm_{0.15}Ca_{0.05}O_{2-\delta}$	1275 °C for 4 h	95	6.48×10^{-4} (500 °C)	1.13	[31]
$Ce_{0.8}Sm_{0.2}O_{1.9}$-5%MgO	1100 °C for 10 min	~92	2.76×10^{-2} (650 °C)	0.8	[32]
$Ce_{0.8}$ $Gd_{0.2}O_{1.90}$	1400 °C for 6 h	95	3.25×10^{-2} (800 °C)	0.64	[33]
$Ce_{0.9}$ $Gd_{0.1}O_{1.95}$	1200 °C for 6 h	89	8.48×10^{-2} (650 °C)	0.759	This research
$Ca_{0.02}Gd_{0.08}Ce_{0.9}O_{1.94}$	1200 °C for 6 h	94.26	5.69×10^{-2} (650 °C)	0.692	This research
$Zn_{0.02}Gd_{0.08}Ce_{0.9}O_{1.94}$	1200 °C for 6 h	95.64	6.52×10^{-2} (650 °C)	0.695	This research

conductivity with a value of 2.89 W/m K at 800 °C (was analyzed up to this temperature due to equipment limitations). These findings also fit with the density results. For instance, in the case of pure GDC, its density was lower sintered at 1200 °C; it should be remembered that a lower density translates into a material with pores, where air is present with a very low thermal conductivity (0.02 W/m K). Therefore, this material resulted in a lower thermal conductivity than the same composition sintered at a higher temperature of 1350 °C. In the case of Zn- GDC, its density did not have a big change, and neither did its conductivity. The Ca- GDC sample decreased its thermal conductivity a little with a higher sintering temperature. All values oscillated between 7.63- 2.89 W/m K, and are comparable to those found in the literature for similar compositions[34], which makes them viable for high-temperature applications.

Given that thermal conductivity can be affected by pore volume fraction, morphology, and spatial distribution, the *k* values were adjusted using Equation 3 to determine the thermal conductivity of a fully dense material.

$$k' / k = 1 - 4/3\, ø \quad (3)$$

Where *k* is the thermal conductivity of the fully dense material, *k'* is the conductivity of the measured samples and ø is the porosity fraction of the samples. These normalized results are shown in Figure 5 (c), where a slight increase in all *k* values can be observed.

4. Conclusions

The systems with the general formulas $Gd_{0.1}Ce_{0.9}O_{1.95}$ and $A_{0.02}Gd_{0.08}Ce_{0.9}O_{1.94}$ (where A = Ca and Zn) were successfully synthesized using mechanochemistry in a high-energy planetary mill. XRD analysis indicated a highly disordered fluorite-like structure formed after 20 hours of milling, with crystallinity increasing as the heat treatment temperature rose. SEM

micrographs showed no significant microstructural changes due to variations in chemical composition or sintering temperature. The incorporation of sintering aids significantly improved density from 89% to ~95%, even at lower sintering temperatures such as 1200 °C. Ionic conductivity remained in the same order of magnitude (10^{-2}), while the lowest thermal conductivity (2.89 W/m K at 800 °C) was observed in Ca-GDC sintered at 1350 °C. Importantly, the addition of sintering aids did not negatively impact either conductivity, making these materials promising candidates for applications in LT-SOFCs or TBCs.

5. Acknowledgments

G. Martínez-De la Rosa thanks CONAHCYT for the Ph.D. scholarship (grant 4031931). The authors also thank TecNM (grant 22966.25-P) for financially supporting this research.

6. References

1. Corigliano O, Pagnotta L, Fragiacomo P. On the Technology of Solid Oxide Fuel Cell (SOFC) energy systems for stationary power generation: a review. Sustainability. 2022;14(22):15276. http://doi.org/10.3390/su142215276.
2. Wang H, Du R, Zhai H, Xi G, Wu F. Preparation and electrochemical characterization of Er3+-doped ceria-chloride composite electrolyte for intermediate-temperature solid oxide fuel cells. Ceram Int. 2019;46(3):2677-81. http://doi.org/10.1016/j.ceramint.2019.09.256.
3. Sreedhar I, Agarwal B, Goyal P, Agarwal A. An overview of degradation in solid oxide fuel cells-potential clean power sources. J Solid State Electrochem. 2020;24(6):1239-70. http://doi.org/10.1007/s10008-020-04584-4.
4. Thakare JG, Pandey C, Mahapatra MM, Mulik RS. Thermal barrier coatings: a state of the art review. Met Mater Int. 2020;27(7):1947-68. http://doi.org/10.1007/s12540-020-00705-w.
5. Trice RW, Su YJ, Mawdsley JR, Faber KT, De Arellano-López AR, Wang H, et al. Effect of heat treatment on phase stability, microstructure, and thermal conductivity of plasma-sprayed YSZ. J Mater Sci. 2002;37(11):2359-65. http://doi.org/10.1023/A:1015310509520.
6. Koettgen J, Martin M. The ionic conductivity of Sm-doped ceria. J Am Ceram Soc. 2020;103(6):3776-87. http://doi.org/10.1111/jace.17066.
7. Steele B. Appraisal of Ce1−yGdyO2−y/2 electrolytes for IT-SOFC operation at 500°C. Solid State Ion. 2000;129(1-4):95-110. http://doi.org/10.1016/S0167-2738(99)00319-7.
8. Puente-Martínez DE, Díaz-Guillén JA, Montemayor SM, Díaz-Guillén JC, Burciaga-Díaz O, Bazaldúa-Medellín ME, et al. High ionic conductivity in CeO2 SOFC solid electrolytes; effect of Dy doping on their electrical properties. Int J Hydrogen Energy. 2019;45(27):14062-70. http://doi.org/10.1016/j.ijhydene.2019.11.032.
9. Malta LFB, Ogasawara T. Degradation of some ceria electrolytes under hydrogen contact nearby anode in solid oxide fuel cells (SOFCs). Mater Res. 2004;7(1):209-13. http://doi.org/10.1590/S1516-14392004000100028.
10. Ocakçı EE, Sarıboğa V, Özdemir H, Altınçekiç TG, Öksüzömer MAF. CA, SR or MG-doped ceria electrolytes prepared by Citrate-Nitrate Combustion Synthesis: effect of doping concentration. J Electroceram. 2023;50(3):67-81. http://doi.org/10.1007/s10832-023-00306-0.
11. Villas-Boas LA, Figueiredo FML, De Souza DPF, Marques FMB. Zn as sintering aid for ceria-based electrolytes. Solid State Ion. 2013;262:522-5. http://doi.org/10.1016/j.ssi.2013.11.002.
12. Kırkgeçit R, Torun HÖ, Dokan FK, Öztürk E. Investigation of photochemical properties of La-Er/CeO2 and La-Y/CeO2 composites. J Photochem Photobiol Chem. 2021;423:113602. http://doi.org/10.1016/j.jphotochem.2021.113602.
13. Tan J, Zhang W, Lv YH, Xia AL. Facile preparation of Mn-doped CeO2 Submicrorods by composite-hydroxide-salt-mediated approach and their magnetic property. Mater Res. 2013;16(4):689-94. http://doi.org/10.1590/S1516-14392013005000040.
14. Vaz ICF, Cabral AC, Procópio AMS, Da Silva Nascimento HM, Amaral DCD, Moura F Fo. Effect synthesis time of CEO2 nanoparticles by Microwave-Assisted hydrothermal as a sensing device on CO gas sensitivity. Mat Res. 2023;26:e20220622. https://doi.org/10.1590/1980-5373-mr-2022-0622.
15. Kim G, Lee N, Kim KB, Kim BK, Chang H, Song SJ, et al. Various synthesis methods of aliovalent-doped ceria and their electrical properties for intermediate temperature solid oxide electrolytes. Int J Hydrogen Energy. 2012;38(3):1571-87. http://doi.org/10.1016/j.ijhydene.2012.11.044.
16. Van Herle J, Horita T, Kawada T, Sakai N, Yokokawa H, Dokiya M. Low temperature fabrication of (Y,Gd,Sm)-doped ceria electrolyte. Solid State Ion. 1996;86-88:1255-8. http://doi.org/10.1016/0167-2738(96)00297-4.
17. Toor SY, Croiset E. Reducing sintering temperature while maintaining high conductivity for SOFC electrolyte: Copper as sintering aid for Samarium Doped Ceria. Ceram Int. 2019;46(1):1148-57. http://doi.org/10.1016/j.ceramint.2019.09.083.
18. Yoshida H, Miura K, Fujita J, Inagaki T. Effect of Gallia addition on the sintering behavior of Samaria-Doped Ceria. J Am Ceram Soc. 1999;82(1):219-21. http://doi.org/10.1111/j.1151-2916.1999.tb01747.x.
19. Maca K, Cihlar J, Castkova K, Zmeskal O, Hadraba H. Sintering of gadolinia-doped ceria prepared by mechanochemical synthesis. J Eur Ceram Soc. 2007;27(13-15):4345-8. http://doi.org/10.1016/j.jeurceramsoc.2007.02.157.
20. Öztürk E, Sarılmaz E. The investigation of the photoluminescent and piezoelectric effect of Eu3+ doped Y2Ti2O7 and Sm2Ti2O7 host crystals. Mater Chem Phys. 2019;239:122085. http://doi.org/10.1016/j.matchemphys.2019.122085.
21. Öztürk E, Kalaycioglu NO, Uzun E. Investigation of luminescence properties of EU3+, DY3+ and GD3+ doped MGAL2SI2O8 red-emitting phosphors. J Chin Chem Soc (Taipei). 2014;62(1):47-51. http://doi.org/10.1002/jccs.201400294.
22. De La Rosa GM, Díaz-Guillén JA. Enhancing densification and electrical properties of Sm-doped ceria with Ca and Zn as sintering aids. Int J Hydrogen Energy. 2023;55:270-6. http://doi.org/10.1016/j.ijhydene.2023.11.290.
23. Shannon RD. Revised effective ionic radii and systematic studies of interatomic distances in halides and chalcogenides. Acta Crystallogr A. 1976;32(5):751-67. http://doi.org/10.1107/S0567739476001551.
24. Mogensen M, Sammes NM, Tompsett GA. Physical, chemical and electrochemical properties of pure and doped ceria. Solid State Ion. 2000;129(1-4):63-94. http://doi.org/10.1016/S0167-2738(99)00318-5.
25. Zhou YC, Rahaman MN. Hydrothermal synthesis and sintering of ultrafine CeO2 powders. J Mater Res. 1993;8(7):1680-6. http://doi.org/10.1557/JMR.1993.1680.
26. Qiu L, Liu F, Zhao L, Ma Y, Yao J. Comparative XPS study of surface reduction for nanocrystalline and microcrystalline ceria powder. Appl Surf Sci. 2005;252(14):4931-5. http://doi.org/10.1016/j.apsusc.2005.07.024.
27. Jonscher AK. Dielectric relaxation in solids. J Phys D Appl Phys. 1999;32(14):R57-70. http://doi.org/10.1088/0022-3727/32/14/201.
28. Puente-Martínez DE, Díaz-Guillén JA, González-García KA, Montemayor SM, Díaz-Guillén JC, Burciaga-Díaz O, et al. Improving the electrical properties of Er-doped CeO2: effect of sintering aids CaO, MgO, and TiO2 on conductivity. J Korean Ceram Soc. 2023;60(5):817-29. http://doi.org/10.1007/s43207-023-00306-4.
29. Jaiswal N, Upadhyay S, Kumar D, Parkash O. Ionic conductivity investigation in lanthanum (La) and strontium (Sr) co-doped

ceria system. J Power Sources. 2012;222:230-6. http://doi.org/10.1016/j.jpowsour.2012.08.095.

30. Ramesh S, Raju KCJ. Structural and ionic conductivity studies of doped ceria electrolyte. Electrochem Solid-State Lett. 2011;15(3):B24. http://doi.org/10.1149/2.019203esl.
31. Srivastava M, Kumar K, Jaiswal N, Singh NK, Kumar D, Parkash O. Enhanced ionic conductivity of co-doped ceria solid solutions and applications in IT-SOFCs. Ceram Int. 2014;40(7):10901-6. http://doi.org/10.1016/j.ceramint.2014.03.086.
32. Xia Z, Meng B, Zhang H, Zheng Q, Liang W, Ping X. Effects of MgO additions on the electrical conduction behavior of a CeO2-based electrolyte prepared by SPS process. Ceram Int. 2019;46(7):9622-8. http://doi.org/10.1016/j.ceramint.2019.12.228.
33. Öksüzömer MAF, Dönmez G, Sariboğa V, Altinçekiç TG. Microstructure and ionic conductivity properties of gadolinia doped ceria (GdxCe1−xO2−x/2) electrolytes for intermediate temperature SOFCs prepared by the polyol method. Ceram Int. 2013;39(7):7305-15. http://doi.org/10.1016/j.ceramint.2013.02.069.
34. Mangalaraja RV, Ananthakumar S, Paulraj M, Pesenti H, López M, Camurri CP, et al. Electrical and thermal characterization of Sm3+ doped ceria electrolytes synthesized by combustion technique. J Alloys Compd. 2011;510(1):134-40. http://doi.org/10.1016/j.jallcom.2011.09.016.